IEEE Access
Multidisciplinary | Rapid Review | Open Access Journal

Received August 5, 2019, accepted September 6, 2019, date of publication September 23, 2019, date of current version October 3, 2019.

Digital Object Identifier 10.1109/ACCESS.2019.2942838

Enhanced Drowsiness Detection Using Deep Learning: An fNIRS Study

M. ASJID TANVEER[1], M. JAWAD KHAN[1], M. JAHANGIR QURESHI[2], NOMAN NASEER[2], (Senior Member, IEEE), AND KEUM-SHIK HONG[3], (Fellow, IEEE)

[1]School of Mechanical and Manufacturing Engineering, National University of Science and Technology, Islamabad 44000, Pakistan
[2]Department of Mechanical Engineering, Air University, Islamabad 44000, Pakistan
[3]School of Mechanical Engineering, Pusan National University, Busan 46241, South Korea

Corresponding author: Keum-Shik Hong (kshong@pusan.ac.kr)

This work was supported by the National Research Foundation (NRF) of South Korea through the Auspices of the Ministry of Science and ICT, South Korea, under Grant NRF-2017R1A2A1A17069430.

ABSTRACT In this paper, a deep-learning-based driver-drowsiness detection for brain-computer interface (BCI) using functional near-infrared spectroscopy (fNIRS) is investigated. The passive brain signals from drowsiness were acquired from 13 healthy subjects while driving a car simulator. The brain activities were measured with a continuous-wave fNIRS system, in which the prefrontal and dorsolateral prefrontal cortices were focused. Deep neural networks (DNN) were pursued to classify the drowsy and alert states. For training and testing the models, the convolutional neural networks (CNN) were used on color map images to determine the best suitable channels for brain activity detection in 0∼1, 0∼3, 0∼5, and 0∼10 second time windows. The average accuracies (i.e., 82.7, 89.4, 93.7, and 97.2% in the 0∼1, 0∼3, 0∼5, and 0∼10 sec time windows, respectively) using DNNs from the right dorsolateral prefrontal cortex were obtained. The CNN architecture resulted in an average accuracy of 99.3%, showing the model to be capable of differentiating the images of drowsy/non-drowsy states. The proposed approach is promising for detecting drowsiness and in accessing the brain location for a passive BCI.

INDEX TERMS Drowsiness detection, functional near-infrared spectroscopy, deep neural network, convolutional neural network, brain-computer interface.

I. INTRODUCTION

Drowsiness has been one of the leading causes of injuries or fatalities in car accidents [1]. Previous research indicates that 10∼30% of car crashes occur owing to driver fatigue or drowsiness [2], [3], which are caused mostly by sleep deprivation [4], intoxication, drug abuse, heat exposure, or/and alcohol [5]. Drowsy drivers have a higher car crash rate than awake individuals [6]. Drowsiness is considered a passive brain phenomenon that does not involve any intension from the subject. In this paper, an improvement of drowsiness detection using functional near-infrared spectroscopy and deep learning algorithms is investigated.

In the past, multiple methods have been devised for the detection of drowsiness. These methods include recording behavior [7], driver physiological signal measurement [8], and vehicle-based performance evaluation [9]. Among these methods, the bio-signal measurement approach showed the highest capability of detecting driver drowsiness: As unlike the other two methods, it depends solely on the driver's condition. Multiple forms of data exist for driver physiological signal measurement, e.g., the detection of neural electrical activity using electroencephalography (EEG), heart rate detection using electrocardiography (ECG), muscle activity utilizing electromyography (EMG), eye movement and blink detection using electrooculography (EOG), and brain hemodynamic change measurement using fNIRS [10].

A brain-computer interface (BCI) is a methodology used for monitoring, communication, and control via signals generated through brain activities. Noninvasive BCI research can be divided into three main categories: Active, reactive, and passive brain tasks [11]. BCI methods measure brain activities using two different types of brain signals; the hemodynamic responses like functional magnetic resonance imaging (fMRI) and fNIRS [12]–[18] or electrophysiological signals like EEG, EMG, and EOG [19]–[21]. The former is produced when blood releases an increased concentration of glucose to activated neurons from the surrounding

The associate editor coordinating the review of this manuscript and approving it for publication was Javier Medina.

This work is licensed under a Creative Commons Attribution 4.0 License. For more information, see http://creativecommons.org/licenses/by/4.0/

region [12], [13]. The latter is produced when neuronal firing occurs due to a brain task [20]. Earlier studies have mostly used EEG [22]–[25] for drowsiness detection, but later some studies using fNIRS were performed either alone or in conjunction with EEG [10], [26], and a few studies using a combination of EEG/ECG/fNIRS [27].

fNIRS in comparison to other brain imaging modalities is relatively low cost, portable, safe, higher temporal resolution (compared to fMRI), and easier to use (unlike magneto encephalography (MEG)). fNIRS is not susceptible to electrical noise as it uses optical signals to acquire brain activities [15], [28]. However, it has some shortcomings, as it has low spatial resolution than fMRI and low temporal resolution compared to EEG [28], [29]. As such fNIRS has some limitations; however, its advantages generally outweigh its disadvantages. fNIRS-BCI have already been used in multiple studies [30]–[32] for various applications such as the classification of prefrontal regions, gait rehabilitation, and motor execution. Also, fNIRS-BCI is used for helping patients with severe congenital motor impairments [33], [34], working memory monitoring of aircraft pilots [35], [36], and speech recognition [37]. Considering the broad applications of fNIRS-BCI, it makes a powerful tool for further research.

Multiple algorithms have been used to classify features between drowsy/non-drowsy states. Most of these algorithms have used machine learning techniques to decipher between the two states [10], [22], [24]–[27], which consist of classifiers such as linear discriminant analysis (LDA), independent component analysis (ICA), k-nearest neighbors (KNN), and most commonly support vector machine (SVM). Two essential steps required when using machine learning algorithms to classify different states is feature selection and feature extraction [38]. Most studies have used a variety of features for this purpose, including frontal beta band relative power level (RPL), HbO changes [10], mean ΔHbO, signal peak, sum of peaks [26], and beat-to-beat (RR-peak) for ECG recording as RR-peaks measure the time for normal and unstable heartbeats [27]. However, these algorithms require manual feature extraction, leaving it up to each study to ensure that the features are appropriate for the classification task. However, deep learning does not require this manual work.

Deep learning approach has been consistently increasing in popularity due to its ability to automate the feature selection and extraction processes; otherwise, they are done manually [39]–[42]. Also, the models employed in deep learning not only extract features but are also able to learn from the features with distinguishable qualities allowing for different purposes (i.e., classification, detection, and segmentation.). Two examples of architectures used in deep learning are convolutional neural networks (CNN) and deep neural networks (DNN). CNNs are commonly trained for classification between images [43]–[46] and consist of convolutional layers for feature extraction from images, with fully connected layers at the end; as such, these models can be used for extracting distinguishing features between labeled images. DNNs consist of multiple neurons, with each neuron attached to every neuron in the layer before and after it and a ''weight'' value determining the use of the neuron to the architecture [47], [48]. These weights are updated during the training phase of the model to enable DNNs to extract useful features.

In this study, we investigate the possibility of detecting a drowsiness state for a passive BCI using the hemodynamic response caused by drowsiness. Signals are measured from the prefrontal and dorsolateral prefrontal cortex brain regions. For this, fNIRS is used to classify between drowsy/non-drowsy states using four windows. The deep learning architectures, DNN, and CNN, are used for feature extraction and evaluation. To our knowledge, this is the first fNIRS investigation that has used the right dorsolateral prefrontal cortex to classify between the passive drowsiness and alert states of a driver by using deep learning architectures, providing very high real-time accuracies. In [49], an extensive review was done over multiple algorithms for BCI. The article has mentioned deep learning algorithms such as recurrent neural networks (RNNs) or long short term memory (LSTM) can be more effecitive for BCI. Deep learning is suitable for brain activity detection (e.g., drowsiness detection, fatigue, etc.). However, given the complexity of these algorithms, it is challenging to implement the algorithm for real-time scenarios. From this view, less complicated methodologies, DNN, and CNN, are applied due to its low computation.

The remainder of this paper is arranged as follows. Section II discusses the methodology used for the extraction of data from subjects and the architectures used for detecting drowsiness, Section III discusses the results obtained during this study, Section IV shows a discussion and comparison with other studies, and Section V concludes the paper.

II. MATERIALS AND METHODS

This section addresses the methodology used to extract data from the subjects, the sensor placement, the signal processing, and the model architecture used in this study. Fig. 1 shows the steps to accomplish these goals.

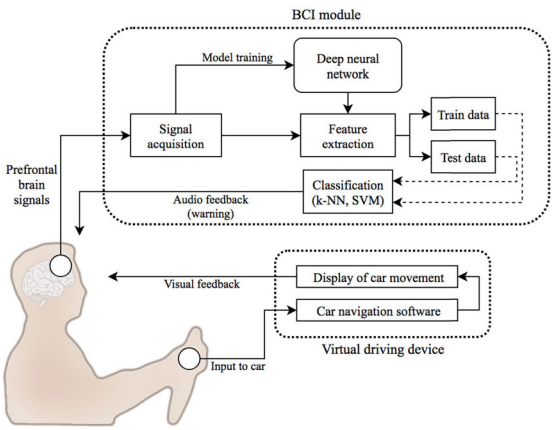

FIGURE 1. Experimental flowchart for drowsiness detection.

A. EXPERIMENTAL PROCEDURE

We used the data set from the work of Khan and Hong [26]. In the experiment, each subject was asked to drive a car driving simulator while sleep deprived. A biomarker was placed in the data when the subject's facial expression changed due to fatigue and sleep loss. The data were recorded for 13 subjects (all male, mean age: 28.5 ± 4.8), among which two were left-handed.

B. SENSOR CONFIGURATION

The optode configuration (Fig. 2) shows how the fNIRS signals are acquired using seven sources and 16 detectors resulting in a combinational pair of 28 channels that are placed on the PFC and dorsolateral prefrontal cortex (DPFC) according to the international 10-20 system [50], [51]. Channels 1∼8 were collected from the right DPFC, labeled as Region A. Channels 9∼20 were collected from the prefrontal cortex, labeled as Region B, and channels 21-28 were obtained from the left dorsolateral prefrontal cortex, labeled as Region C.

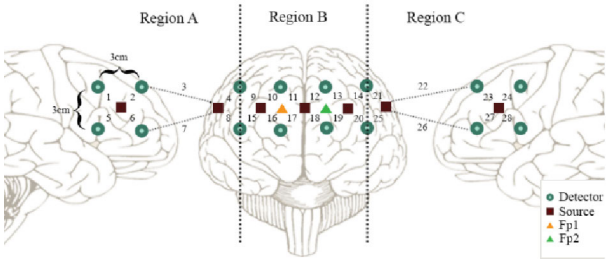

FIGURE 2. Optodes placement over the prefrontal and dorsolateral prefrontal cortices [26].

C. SIGNAL ACQUISITION AND PROCESSING

A continuous wave-imaging system (DYNOT, NIRx, Medical Technologies, USA) was used to record brain signals at 760 and 830 nm wavelengths. Data were collected at a sampling rate of 1.81 Hz. Gaussian filters were applied to remove heartbeat, respiratory, and other motion noise from the data [52]–[56]. Raw intensity values were converted to oxygenated and deoxygenated hemoglobin concentration changes (i.e., ΔHbO and ΔHbR) using the modified Beer-Lambert law [57] given as

$$A\,(t;\lambda) = \ln\frac{I_{in}\,(\lambda)}{I_{out}\,(t;\lambda)} = \alpha\,(\lambda)\times c(\lambda)\times l\times d(\lambda)+\eta, \tag{1}$$

$$\begin{bmatrix}\Delta c_{HbO}(t)\\ \Delta c_{HbR}(t)\end{bmatrix} = \begin{bmatrix}\alpha_{HbO}(\lambda_1) & \alpha_{HbR}(\lambda_1)\\ \alpha_{HbO}(\lambda_2) & \alpha_{HbR}(\lambda_2)\end{bmatrix}^{-1}\begin{bmatrix}\Delta A\,(t;\lambda_1)\\ \Delta A(t;\lambda_2)\end{bmatrix}\frac{1}{l\times d(\lambda)}. \tag{2}$$

Here A defines the absorbance of light (optical density), I_{in} is the incident intensity, and I_{out} is the detected intensity of light. Additionally, α is the specific extinction coefficient in $\mu\text{M}^{-1}\text{cm}^{-1}$, c is the absorber concentration in μM, l is the distance between the source and detector in cm, d is the differential path-length factor, and η is the loss of light due to scattering.

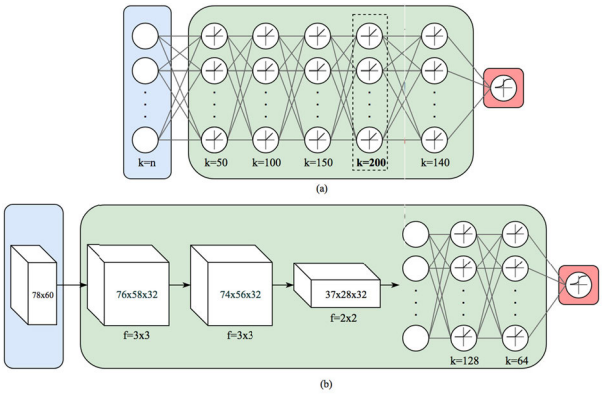

FIGURE 3. DNN model used for classification purposes. The dotted line around layer k = 200 shows layers extracted later for feature extraction; (b) CNN model used for channel drowsiness activity through image classification.

D. MODEL ARCHITECTURE

Deep learning architectures have proven to be a powerful tool regarding classification purposes. In this study, two deep learning architectures were used [58]–[60]: One was used for classifying between drowsy/alert states, i.e., DNN, and the other was used for detecting the strength of each channel for detecting tired case, i.e., CNN. One important parameter to consider is the size of data in time. In this study, four different window sizes were used (i.e., 0∼1, 0∼3, 0∼5, and 0∼10 seconds). Time-domain signals were used only for the classification task; to detect the strength of a channel in identifying the drowsy state, the data of a time window depicting all the channels were converted to a color map. Thus, each subject will have 28 different color maps for each time window.

For DNN, the input size shown as parameter "n" (Fig. 3(a)) was decided based on the window size. The hidden layers section consists of dense layers; the starting layer had 50 neurons, and the ending layer had 200 neurons. A 30% dropout was introduced before the output layer to prevent overfitting. The model was trained based on the labeled input passed through the neural network, and the final hidden layer before dropout was used to extract features for each time window, which were fed into the KNN classifier to train and test the data using 10-fold cross-validation.

The CNN architecture was used for the classification of the color map images created from each time window for all channels. Fig. 3(b) shows the model architecture starting with the input; all input images were the same size (78 × 60) and were passed through the neural network for training. The hidden layers consisted of two convolution filters with a size of (3 × 3) applied on the input images, followed by a max-pooling layer with a size of (2 × 2). This was done to reduce the input feature size and retain only robustt features.

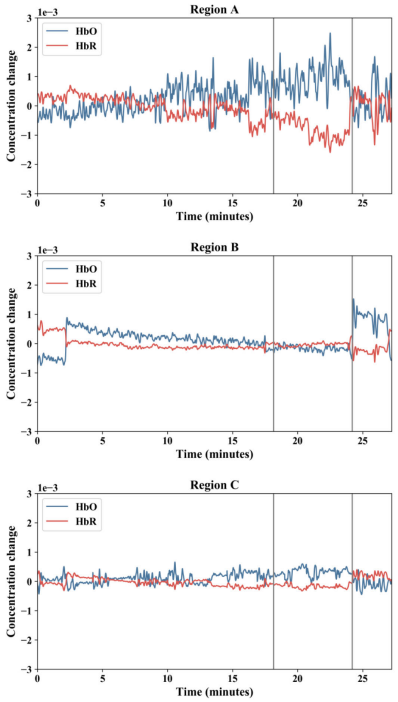

FIGURE 4. Comparison between average signal at each region (A, B and C), showing drowsy and alert state (Subject 5) [26].

The features were then converted to a fully connected layer and passed through a dense layer with 128 neurons, and a 50% dropout was introduced before the output layer to prevent overfitting of the model.

The ReLu activation function was used in the hidden layers as follows.

$$R(z) = \max(0, z). \tag{3}$$

R(z) shows the output ReLu function, while z shows the weighted sum of the input parameters to each neuron. The function returns zero if the weighted sum is less than zero, and z is returned if the weighed sum is greater than or equal to zero. A sigmoid activation function was used for the output layers as follows.

$$\sigma(z) = \frac{1}{1 + e^{-z}} \tag{4}$$

In this equation, $\sigma(z)$ shows the sigmoid output function, and z shows the weighted sum of input parameters. Activation function plots can be seen within each layer (see Fig. 3). Binary cross-entropy is used as a loss measure and is minimized during training.

$$BCE = -\frac{1}{N}\sum_{i=0}^{N} y_i * \log(y_i^o) + (1 - y_i) * \log(1 - y_i^o) \tag{5}$$

where N shows the total number of training examples, and y_i shows the labeled output (i.e., 0 and 1 in the case of binary classification), while y_i^o shows the output generated by the model during training.

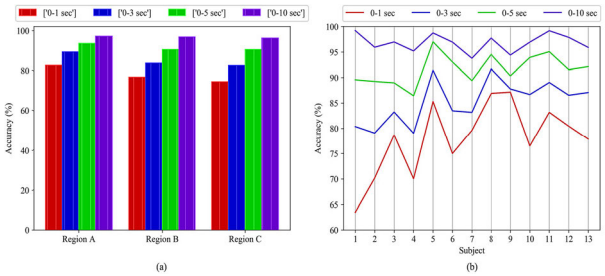

FIGURE 5. (a) Average classification accuracy (%) on overall 13 subjects in each time window. (b) Average subject classification accuracy at each time window.

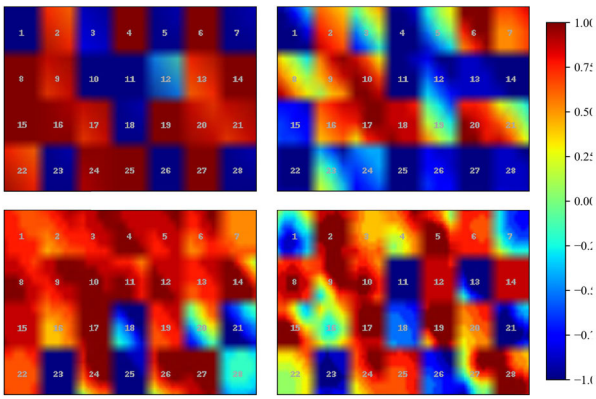

FIGURE 6. Color maps for 28 channels at different time windows (0∼1, 0∼3, 0∼5, and 0∼10 seconds). Numbers in the color maps indicate individual channels (Subject 6).

III. RESULTS

The data for each subject were divided into three separate regions (Fig. 4), and for each subject, the respective channels in these regions were averaged to create a single signal for each region (i.e., A, B and C). Region A shows the strongest drowsiness activity compared to Regions B and C. Fig. 4 shows hemodynamic changes in the three regions.

The signals were then segmented into smaller time windows; for example, a 30 min signal, if segmented into a 0∼1 sec time window, will result in a total of 1,800 values (30 × 60). Similarly, there will be 600, 360, and 180 total values for 0∼3 sec, 0∼5 sec, and 0∼10 sec windows. After these segments were acquired, they were passed through the DNN with the model trained to classify between drowsy and non-drowsy states.

The model was trained for 200 epochs, after which the final hidden layer before the dropout was used to extract features from each segment, resulting in 200 features per segment. Table 1 shows the classification accuracies of the individual subjects at each time window.

Fig. 5(a) shows the individual regional performances for the different time windows, showing that Region A has the highest overall performance, especially in the smaller time windows. The average subject performance in each region was also evaluated; for each subject, the performance in each region for the 4-time windows was averaged and is plotted in Fig. 5(b).

TABLE 1. Classification accuracies (%) in three different brain regions.

	Region A				Region B				Region C			
Subjects	0~1 (s)	0~3 (s)	0~5 (s)	0~10 (s)	0~1 (s)	0~3 (s)	0~5 (s)	0~10 (s)	0~1 (s)	0~3 (s)	0~5 (s)	0~10 (s)
1	66.5	84.8	92.4	100.0	65.5	83.7	88.8	99.4	58.3	72.6	87.5	98.2
2	67.7	85.2	95.9	100.0	58.3	64.3	81.8	99.0	84.5	87.7	90.0	88.8
3	87.6	88.1	91.6	93.8	89.9	90.4	92.0	98.5	58.5	71.2	83.3	98.6
4	82.5	94.6	99.4	100.0	68.1	78.2	83.4	92.6	59.5	64.3	76.5	93.0
5	80.4	89.8	97.3	100.0	92.0	94.9	97.5	98.2	83.5	89.6	96.2	98.0
6	86.5	88.8	97.2	92.6	59.4	76.8	90.5	100	79.1	84.8	91.4	98.2
7	88.3	90.2	91.1	92.9	79.3	84.3	89.9	93.7	71.2	75.0	87.2	94.7
8	89.4	93.4	95.7	96.2	84.8	92.6	94.6	98.8	86.5	89.2	93.4	98.3
9	90.1	90.2	91.5	98.9	84.6	85.6	89.1	88.5	86.7	87.5	90.4	95.8
10	85.5	87.4	88.9	96.2	71.2	84.4	96.2	100.0	72.8	88.2	96.7	94.6
11	80.1	89.7	94.9	99.0	84.4	87.3	94.4	100.0	85.0	90.1	95.9	98.5
12	80.7	84.9	86.2	95.3	83.3	87.4	91.9	99.4	77.3	87.3	96.5	98.9
13	90.1	95.2	95.7	99.3	77.9	79.9	88.1	91.4	65.6	86.1	92.6	97.0
Mean	82.7	89.4	93.7	97.2	76.8	83.8	90.6	96.8	74.5	82.5	90.5	96.3

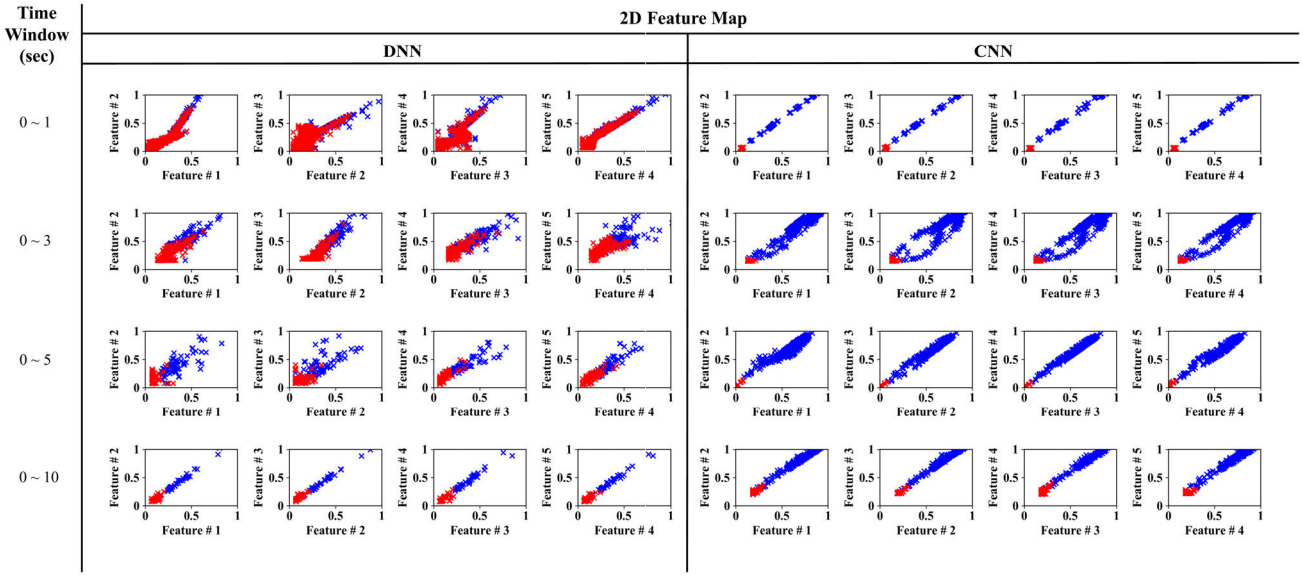

FIGURE 7. 2-class feature spaces for DNN and CNN at each time window (Subject 5).

The color maps generated for two separate time windows (Fig. 6) distinctly show each channel, with the channel numbers given in the center of each color map. To generate color maps, the signals were segmented into shorter time windows, and then, for each time window, a color map was generated for the entire channels. For example, the segmentation of a 30 min signal with 0∼10 sec time windows result in 180 segments. This results in 5,040 (180 × 28) color maps for all signals. To distinguish between drowsy and non-drowsy states, the mean values were generated for all channels, followed by averaging across all 28 means. This new average was used to label segments from each channel; if a segment value was above the mean, it was labeled as drowsy, while signals below the mean were considered non-drowsy.

After generating the labeled color map data, a 50-40-10 (Train-Test-Validation) ratio was used to train and test the model in Fig. 3(b) for ten epochs across each subject, resulting in an average test accuracy of 99.3%. This result shows that the model is very susceptible to drowsy/non-drowsy detection. To better understand the skills of the two models, Fig. 7 illustrates a 2D feature space using combinations of two features (Subject 5). Given the large number of features available for each model, feature selection was used to extract the top 5 features for each model, at each time window. As seen from Fig. 7, DNN performs better in a full time window in comparison to a small time window for drowsiness detection. The increase of accuracy by increasing the window size using DNN is shown in Table 1. In comparison to DNN, CNN uses (brain) images for classification. Therefore, it can distinguish the two states (i.e., tired and non-drowsy) at a lower time window. Both models had relatively small computation time (see Table 2) at each time window, using a 20% test dataset. For DNN, the computation time was measured in the absence of KNN. A sigmoid activation function is used at the output layer. Also, the CNN model took a considerably longer to compute than the DNN model at each time window, possibly due to more data available for CNN models (since all 28 channels were used together), different

TABLE 2. Computation time taken by each model.

	DNN (Computation time (sec))				CNN (Computation time (sec))			
Subjects	0~1	0~3	0~5	0~10	0~1	0~3	0~5	0~10
1	0.032	0.025	0.024	0.023	1.7	0.68	0.42	0.17
2	0.034	0.028	0.025	0.023	1.9	0.69	0.38	0.20
3	0.034	0.028	0.025	0.024	2.0	0.82	0.41	0.19
4	0.032	0.027	0.024	0.025	1.6	0.66	0.36	0.15
5	0.033	0.028	0.024	0.025	1.6	0.63	0.35	0.16
6	0.034	0.030	0.024	0.024	2.0	0.77	0.38	0.19
7	0.034	0.026	0.026	0.024	2.2	0.85	0.43	0.23
8	0.033	0.028	0.025	0.023	1.9	0.73	0.38	0.16
9	0.033	0.027	0.024	0.024	1.7	0.64	0.34	0.16
10	0.032	0.029	0.025	0.023	1.7	0.69	0.38	0.13
11	0.034	0.028	0.026	0.025	2.1	0.89	0.41	0.19
12	0.032	0.027	0.024	0.025	1.9	0.77	0.42	0.19
13	0.032	0.025	0.025	0.024	2.1	0.82	0.43	0.22
Mean	0.033	0.027	0.025	0.024	1.8	0.74	0.39	0.18

Note: Nvidia 1060 Gtx was used for the models. Given different GPUs the computation time could change.

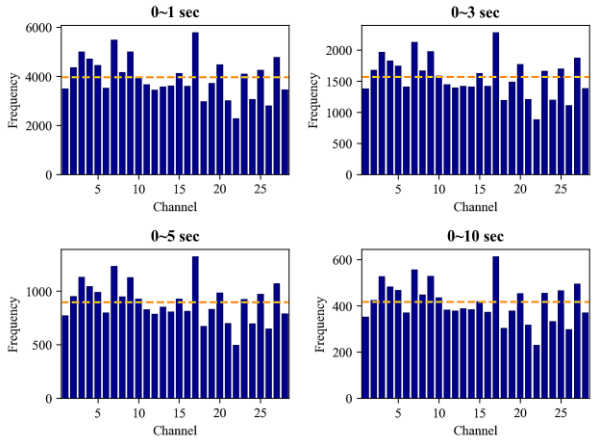

FIGURE 8. Channel wise occurrence of drowsy state through all subjects. The orange line indicates mean frequency value.

batch sizes used for each model and the difference in hidden layers among the models. It is worth mentioning that individual machine specifications can alter the testing/computation time taken by each model.

Using the model, the frequency of drowsiness was measured across all channels at each time window (refer to Fig. 8); the mean frequency at each time window was used to detect the channels showing the most substantial presence of the drowsy state. Channels with frequencies above the mean across all time windows were considered the most reliable candidates (i.e., channels 2, 3, 4, 5, 7, 8, 9, 15, 17, 20, 23, 25 and 27). To test whether these channels show a better performance than the other channels, a new region was created (i.e., Region X) consisting of the most active candidate channels. An average signal was generated using these 13 channels and passed through the model in Fig. 3(a). Table 3 shows the classification accuracy for this region across all subjects, as well as a comparison between the used KNN and SVM classifiers. Performance was compared for two measures (i.e., accuracy (%) and computation time (sec)).

It can be seen that a higher average performance was achieved in the new region than in Region A, indicating that the selected channels are indeed a better choice than the other channels for drowsy/non-drowsy classification. Additionally, a higher performance was observed for SVM than for KNN; however, the difference in the performance was minimal compared to the high computation time of SVM. This proves that, given real-time scenarios, KNN would be better for drowsiness detection than SVM due to its substantially lower computation time.

IV. DISCUSSION

In the previous literature concerning vigilance [26], [61], a significant peak occurred in the event-related hemodynamic response between 5∼8 and 0∼5 sec time windows. However, the present work enables us to detect vigilance in a 0∼1 sec time window, thereby reducing the time taken to alert the driver of his or her current status.

The previous works on fNIRS have used manual feature extraction methods for their machine learning algorithms [26], [27], [62], [63], e.g., the mean of ΔHbO/ΔHbR, signal peaks and signal slopes. However, deep learning architectures remove the need for manual feature extraction and automate the process; learning from examples, a deep learning architecture extracts its own set of features. In doing so, high amounts of time and effort are saved that would otherwise be spent on determining the feature requirements to improve the classification result.

This study shows that among three regions (i.e., right DPFC, PFC, and left DPFC), the right DPFC shows the highest classification accuracy between the drowsy/non-drowsy states, with accuracies varying from 97.2 to 74.5% from right to left in the PFC region within 0∼10 to 0∼1 sec time windows. Besides, the new Region X shows higher classification accuracy than Region A. The significance of the obtained accuracies for real-time computation was computed using the *t*-test. The accuracy obtained in Region A was compared with the accuracies obtained in Regions B and C for small time windows (i.e., 0∼1 and 0∼3 sec). The *p*-values obtained for Region A vs. Region B were 0.04 and 0.02, while those for Region A vs. Region C were 0.03 and 0.01. This shows that the results obtained are very significant and that Region A proves to be the most suitable region for real-time detection of drowsy state.

In the previous work [26] performed on Region A using the same dataset, an accuracy of 83.4% for 0∼10 sec window was reported, while an accuracy of 83.1% was reported for the smallest time window of 0∼5 sec. The proposed study achieves an accuracy of 97.2% for the 0∼10 sec window and an accuracy of 82.7% for the smallest time window, 0∼1 sec. The current work surpasses the previous work in terms of both accuracy and real-life implementation, giving higher accuracies at small time windows. Another study [10] used a hybrid EEG/fNIRS system to predict driver drowsiness, reporting an accuracy of 70.5% for EEG, 73.7% for NIRS, and 79.2% for combined EEG/NIRS.

TABLE 3. Performance evaluation of new region; and comparison between KNN and SVM.

	KNN (accuracy (%) / computation time (sec))				SVM (accuracy (%) / computation time (sec))			
Subjects	0~1 (s)	0~3 (s)	0~5 (s)	0~10 (s)	0~1 (s)	0~3 (s)	0~5 (s)	0~10 (s)
1	68.9/0.05	86.7/0.012	96.1/0.005	99.4/0.002	72.6/0.46	88.7/0.04	95.7/0.012	100.0/0.002
2	67.8/0.06	84.5/0.015	94.7/0.006	100.0/0.002	72.7/0.54	88.1/0.05	94.1/0.009	100.0/0.002
3	88.1/0.04	88.7/0.012	92.3/0.005	96.2/0.002	88.6/0.31	90.1/0.04	92.5/0.013	96.2/0.005
4	83.5/0.06	93.2/0.012	99.4/0.005	100.0/0.002	85.1/0.25	93.8/0.03	100.0/0.007	100.0/0.003
5	79.7/0.05	90.7/0.013	98.8/0.005	100.0/0.002	81.5/0.23	89.1/0.02	97.8/0.007	99.4/0.002
6	85.2/0.04	93.9/0.011	97.8/0.004	96.3/0.002	87.2/0.18	91.2/0.02	97.5/0.006	98.0/0.003
7	88.2/0.04	88.3/0.012	92.6/0.005	91.4/0.002	89.1/0.24	89.9/0.03	91.3/0.014	92.4/0.004
8	89.8/0.03	93.2/0.012	94.4/0.005	96.8/0.002	90.7//0.20	93.3/0.02	95.9/0.008	98.3/0.003
9	90.3/0.04	90.6/0.011	94.6/0.004	98.4/0.002	91.3/0.16	91.9/0.02	93.8/0.009	97.3/0.002
10	83.8/0.03	89.4/0.009	91.1/0.004	91.8/0.002	86.5/0.25	89.7/0.04	93.0/0.011	95.7/0.003
11	84.7/0.05	90.7/0.013	93.9/0.006	99.5/0.003	87.3/0.26	89.5/0.03	93.8/0.008	100.0/0.002
12	83.1/0.03	85.1/0.009	86.1/0.004	96.0/0.002	86.7/0.18	86.8/0.03	87.0/0.012	93.1/0.003
13	90.7/0.03	95.1/0.010	97.9/0.004	97.5/0.002	91.8/0.14	95.6/0.01	97.8/0.005	99.3/0.002
Mean	83.3/0.04	89.9/0.011	94.5/0.004	97.1/0.002	85.5/0.26	90.6/0.03	94.6/0.009	97.6/0.003

TABLE 4. Performance comparison between the proposed method and previous studies.

Authors	Modality	Features	Classifier	Accu (%)
Chuang et al. [25]	EEG	Nonparametric weighting feature extraction (NWFE)	Radial basis function neural network (RBFNN)	91.6
Khan and Hong [26]	fNIRS	Mean of ΔHbO, signal peak, sum of peaks	Linear discriminant analysis (LDA)	83.1
Nguyen et al. [10]	EEG/ fNIRS	Frontal beta band RPL, ΔHbO change	Fisher's linear discriminant analysis (FLDA)	79.2
Ahn et al. [27]	EEG/ ECG/ fNIRS	Relative power level/ RR-peak interval/ ΔHbO change	Fisher's linear discriminant analysis (FLDA)	75.9
Zhang et al. [24]	EEG	PSD of frequency components	Support vector machines (SVM)	84.1
Wei et al. [64]	EEG	Pre-event logarithmic theta, alpha and beta powers	Support vector machines (SVM)	87.6
Proposed method	fNIRS	Deep learning extracted features	K nearest neighbors (KNN)	83.3

Additionally, in [23], an EOG/EEG system was developed to detect driver drowsiness using parameters such as blink duration, and accuracies of 93% for binary and 79% for multiclass classification were achieved; however, the higher accuracy of this previous study compared to the current study can be explained by the use of different modalities, which result in a slower algorithm. In addition, Ahn *et al.* [27] used EEG/ECG/fNIRS and reported the highest accuracy of 75.9% when all signals were combined and an accuracy of 66.8% when purely fNIRS was used. The proposed method achieves higher accuracy than the methods of previous studies at a lower window size (0∼1 sec), resulting in higher accuracy with better real-time implementation. Another study using variable time windows [24] showed an average accuracy of 84.1% for the occipital site (O2) in the 0∼1 sec time window. Though higher in accuracy, the study suffered from an average high testing time of 1.3 sec; in contrast, the testing time of the present study was 0.05 sec. Research [25] showed promising results, with an accuracy of 91.6% with a 0∼1 sec window; however, its results were obtained with only four subjects, whereas the proposed study worked on 13 subjects, resulting in a decreased confidence in the results due to the greater number of subjects used. Also, Wei *et al.* [64] showed a higher performance compared to the current study; however, the use of SVMs will result in a slower algorithm, unfit for real-time application. Table 4 summarizes the comparisons made between the proposed research and the previous studies. Previous researches have also used Bayesian-copula discriminant classifier (BCDC) and Bayesian nonnegative CP decomposition (BNCPD) for drowsiness detection using EEG [65], [66]. The highest achieved accuracy using BCDC and BNCPD was 94.3% and 84.12%, respectively, using a 5 sec time window. The current study has similar results in comparison to BCDC; however, the proposed algorithm performs better than the BNCPD algorithm. The sampling rate for both studies [65], [66] was 100 Hz. In comparison, we have achieved the same accuracy using 1.81 Hz sampling rate. Also, the proposed window size by the previous algorithms is 5 sec, whereas our method can detect drowsiness in 1-sec window. Another study has used the hidden Markov models in combination with Bayesian networks for fatigue detection achieving an accuracy of 98.4% [67]: However, the use of long time windows makes the study less applicable for real-time scenarios.

The results of the current study clearly show a drastic improvement from the previous research. This work belongs to the category of sole fNIRS-BCI to perform classification of the alert and drowsy states using the hemodynamic response and uses spatial filtering by segmenting the prefrontal brain region to identify the region of interest for drowsiness detection.

V. CONCLUSION

This study investigated the potential of drowsiness detection using deep learning algorithms and functional near-infrared spectroscopy for a passive brain-computer interface. A deep neural network was used to detect driver drowsiness using four windows (0∼1, 0∼3, 0∼5, and 0∼10). We also used the convolutional neural network on the functional brain maps, giving an accuracy of 99.3%, and found thirteen distinct channels that are most active during drowsiness, as well as a new region consisting of the channels that showed the highest classification accuracy.

REFERENCES

[1] K. Fujiwara, E. Abe, K. Kamata, C. Nakayama, Y. Suzuki, T. Yamakawa, T. Hiraoka, M. Kano, Y. Sumi, F. Masuda, M. Matsuo, and H. Kadotani, "Heart rate variability-based driver drowsiness detection and its validation with EEG," *IEEE Trans. Biomed. Eng.*, vol. 66, no. 6, pp. 1769–1778, Jun. 2019.

[2] K. Ismail, T. Sayed, N. Saunier, and C. Lim, "Automated analysis of pedestrian-vehicle conflicts using video data," *Transp. Res. Rec. J. Transp. Res. Board*, vol. 2140, no. 1, pp. 44–54, Dec. 2009.

[3] P. Philip and T. Åkerstedt, "Transport and industrial safety, how are they affected by sleepiness and sleep restriction?" *Sleep Med. Rev.*, vol. 10, no. 5, pp. 347–356, Oct. 2006.

[4] C. F. P. George, "Sleep apnea, alertness, and motor vehicle crashes," *Amer. J. Respiratory Crit. Care Med.*, vol. 176, no. 10, pp. 954–956, Nov. 2007.

[5] J. A. Owens, T. Dearth-Wesley, A. N. Herman, and R. C. Whitaker, "Drowsy driving, sleep duration, and chronotype in adolescents," *J. Pediatrics*, vol. 205, pp. 224–229, Feb. 2019.

[6] J. Vicente, P. Laguna, A. Bartra, and R. Bailon, "Drowsiness detection using heart rate variability," *Med. Biol. Eng. Comput.*, vol. 54, no. 6, pp. 927–937, 2016.

[7] Q. Ji and X. Yang, "Real-time eye, gaze, and face pose tracking for monitoring driver vigilance," *Real-Time Imag.*, vol. 8, no. 5, pp. 357–377, 2002.

[8] S. K. L. Lal and A. Craig, "A critical review of the psychophysiology of driver fatigue," *Biol. Psychol.*, vol. 55, no. 3, pp. 173–194, Feb. 2001.

[9] C. C. Liu, S. G. Hosking, and M. G. Lenné, "Predicting driver drowsiness using vehicle measures: Recent insights and future challenges," *J. Saf. Res.*, vol. 40, pp. 239–245, Aug. 2009.

[10] T. Nguyen, S. Ahn, H. Jang, S. C. Jun, and J. G. Kim, "Utilization of a combined EEG/NIRS system to predict driver drowsiness," *Sci. Rep.*, vol. 7, Mar. 2017, Art. no. 43933.

[11] T. O. Zander and C. Kothe, "Towards passive brain–computer interfaces: Applying brain–computer interface technology to human–machine systems in general," *J. Neural Eng.*, vol. 8, no. 2, Apr. 2011, Art. no. 025005.

[12] D. A. Boas, C. E. Elwell, M. Ferrari, and G. Taga, "Twenty years of functional near-infrared spectroscopy: Introduction for the special issue," *NeuroImage*, vol. 85, pp. 1–5, Jan. 2014.

[13] M. Ferrari and V. Quaresima, "A brief review on the history of human functional near-infrared spectroscopy (fNIRS) development and fields of application," *NeuroImage*, vol. 63, no. 2, pp. 921–935, 2012.

[14] N. K. Logothetis, "What we can do and what we cannot do with fMRI," *Nature*, vol. 453, no. 7197, pp. 869–878, 2008.

[15] N. Naseer and K.-S. Hong, "fNIRS-based brain-computer interfaces: A review," *Frontiers Hum. Neurosci.*, vol. 9, Jan. 2015, Art. no. 3.

[16] M. Strait and M. Scheutz, "What we can and cannot (yet) do with functional near infrared spectroscopy," *Frontiers Neurosci.*, vol. 8, Mar. 2014, Art. no. 117.

[17] M. P. van den Heuvel and H. E. H. Pol, "Exploring the brain network: A review on resting-state fMRI functional connectivity," *Eur. Neuropsychopharmacol.*, vol. 20, no. 8, pp. 519–534, 2010.

[18] M. Welvaert and Y. Rosseel, "A review of fMRI simulation studies," *PLoS One*, vol. 9, no. 7, Jul. 2014, Art. no. e101953.

[19] S. Coyle, T. Ward, and C. Markham, "Brain–computer interfaces: A review," *Interdiscipl. Sci. Rev.*, vol. 28, no. 2, pp. 112–118, Jul. 2003.

[20] L. F. Nicolas-Alonso and J. Gomez-Gil, "Brain computer interfaces, a review," *Sensors*, vol. 12, no. 2, pp. 1211–1279, 2012.

[21] A. Turnip, K.-S. Hong, and M.-Y. Jeong, "Real-time feature extraction of P300 component using adaptive nonlinear principal component analysis," *Biomed. Eng. Online*, vol. 10, Sep. 2011, Art. no. 83.

[22] D. Wu, J.-T. King, C.-H. Chuang, C.-T. Lin, and T.-P. Jung, "Spatial filtering for EEG-based regression problems in brain–computer interface (BCI)," *IEEE Trans. Fuzzy Syst.*, vol. 26, no. 2, pp. 771–781, Apr. 2018.

[23] S. Barua, M. U. Ahmed, C. Ahlström, and S. Begum, "Automatic driver sleepiness detection using EEG, EOG and contextual information," *Expert Syst. Appl.*, vol. 115, pp. 121–135, Jan. 2019.

[24] X. Zhang, J. Li, Y. Liu, Z. Zhang, Z. Wang, D. Luo, X. Zhou, M. Zhu, W. Salman, G. Hu, and C. Wang, "Design of a fatigue detection system for high-speed trains based on driver vigilance using a wireless wearable EEG," *Sensors*, vol. 17, no. 3, Mar. 2017, Art. no. 486.

[25] C.-H. Chuang, L.-W. Ko, Y.-P. Lin, Y.-P. Jung, and C.-T. Lin, "Independent component ensemble of EEG for brain–computer interface," *IEEE Trans. Neural Syst. Rehabil. Eng.*, vol. 22, no. 2, pp. 230–238, Mar. 2014.

[26] M. J. Khan and K.-S. Hong, "Passive BCI based on drowsiness detection: An fNIRS study," *Biomed. Opt. Express*, vol. 6, no. 10, pp. 4063–4078, Oct. 2015.

[27] S. Ahn, T. Nguyen, H. Jang, J. G. Kim, and S. C. Jun, "Exploring neuro-physiological correlates of drivers' mental fatigue caused by sleep deprivation using simultaneous EEG, ECG, and fNIRS data," *Frontiers Hum. Neurosci.*, vol. 10, May 2016, Art. no. 219.

[28] T. Wilcox and M. Biondi, "fNIRS in the developmental sciences," *Wiley Interdiscipl. Rev., Cognit. Sci.*, vol. 6, no. 3, pp. 263–283, 2015.

[29] A. Berger, F. Horst, S. Müller, F. Steinberg, and M. Doppelmayr, "Current state and future prospects of EEG and fNIRS in robot-assisted gait rehabilitation: A brief review," *Frontiers Hum. Neurosci.*, vol. 13, Jun. 2019. Art. no. 172.

[30] R. Zimmermann, L. Marchal-Crespo, J. Edelmann, O. Lambercy, M.-C. Fluet, R. Riener, M. Wolf, and R. Gassert, "Detection of motor execution using a hybrid fNIRS-biosignal BCI: A feasibility study," *J. NeuroEng. Rehabil.*, vol. 10, Jan. 2013, Art. no. 4.

[31] M. Rea, M. Rana, N. Lugato, P. Terekhin, L. Gizzi, D. Brötz, and A. Caria, "Lower limb movement preparation in chronic stroke: A pilot study toward an fNIRS-BCI for gait rehabilitation," *Neurorehabilitation Neural Repair*, vol. 28, no. 6, pp. 564–575, Jul. 2014.

[32] K.-S. Hong, N. Naseer, and Y.-H. Kim, "Classification of prefrontal and motor cortex signals for three-class fNIRS–BCI," *Neurosci. Lett.*, vol. 587, pp. 87–92, Feb. 2015.

[33] L. C. Schudlo and T. Chau, "Development and testing an online near-infrared spectroscopy brain–computer interface tailored to an individual with severe congenital motor impairments," *Disab. Rehabil., Assistive Technol.*, vol. 13, no. 6, pp. 581–591, 2018.

[34] L. C. Schudlo and T. Chau, "Development of a ternary near-infrared spectroscopy brain-computer interface: Online classification of verbal fluency task, stroop task and rest," *Int. J. Neural Syst.*, vol. 28, no. 4, May 2018, Art. no. 1750052.

[35] T. Gateau, H. Ayaz, and F. Dehais, "*In silico* vs. over the clouds: On-the-fly mental state estimation of aircraft pilots, using a functional near infrared spectroscopy based passive-BCI," *Frontiers Hum. Neurosci.*, vol. 12, May 2018, Art. no. 187.

[36] K. J. Verdière, R. N. Roy, and F. Dehais, "Detecting pilot's engagement using fNIRS connectivity features in an automated vs. manual landing scenario," *Frontiers Hum. Neurosci.*, vol. 12, Jan. 2018, Art. no. 6.

[37] Y. Liu and H. Ayaz, "Speech recognition via fNIRS based brain signals," *Frontiers Neurosci.*, vol. 12, Oct. 2018, Art. no. 695.

[38] S. Lemm, B. Blankertz, T. Dickhaus, and K.-R. Müller, "Introduction to machine learning for brain imaging," *NeuroImage*, vol. 56, no. 2, pp. 387–399, 2011.

[39] M. Zhang, M. Gong, Y. Mao, J. Li, and Y. Wu, "Unsupervised feature extraction in hyperspectral images based on wasserstein generative adversarial network," *IEEE Trans. Geosci. Remote Sens.*, vol. 57, no. 5, pp. 2669–2688, May 2019.

[40] Y. Yang, Z. Ye, Y. Su, Q. Zhao, X. Li, and D. Ouyang, "Deep learning for *in vitro* prediction of pharmaceutical formulations," *Acta Pharmaceutica Sinica B.*, vol. 9, no. 1, pp. 177–185, Jan. 2019.

[41] M. Usama, B. Ahmad, J. Wan, M. S. Hossain, M. F. Alhamid, and M. A. Hossain, "Deep feature learning for disease risk assessment based on convolutional neural network with intra-layer recurrent connection by using hospital big data," *IEEE Access*, vol. 6, pp. 67927–67939, Nov. 2018.

[42] D. Pei, M. Burns, R. Chandramouli, and R. Vinjamuri, "Decoding asynchronous reaching in electroencephalography using stacked autoencoders," *IEEE Access*, vol. 6, pp. 52889–52898, 2018.

[43] H. Zhang, B. Chen, Z. Wang, and H. Liu, "Deep max-margin discriminant projection," *IEEE Trans. Cybern.*, vol. 49, no. 7, pp. 2454–2466, Jul. 2019.
[44] A.-D. Nguyen, J. Kim, H. Oh, H. Kim, W. Lin, and S. Lee, "Deep visual saliency on stereoscopic images," *IEEE Trans. Image Process.*, vol. 28, no. 4, pp. 1939–1953, Apr. 2019.
[45] Y. Wu, Y. Lin, Z. Zhou, D. C. Bolton, J. Liu, and P. Johnson, "DeepDetect: A cascaded region-based densely connected network for seismic event detection," *IEEE Trans. Geosci. Remote Sens.*, vol. 57, no. 1, pp. 62–75, Jan. 2019.
[46] R. Olmos, S. Tabik, A. Lamas, F. Pérez-Hernández, and F. Herrera, "A binocular image fusion approach for minimizing false positives in handgun detection with deep learning," *Inf. Fusion*, vol. 49, pp. 271–280, Sep. 2019.
[47] X. Cao, Y. Ge, R. Li, J. Zhao, and L. Jiao, "Hyperspectral imagery classification with deep metric learning," *Neurocomputing*, vol. 356, no. 3, pp. 217–227, Sep. 2019.
[48] M. S. Hossain and G. Muhammad, "Emotion recognition using deep learning approach from audio-visual emotional big data," *Inf. Fusion*, vol. 49, pp. 69–78, Sep. 2019.
[49] X. Zhang, L. Yao, X. Wang, J. Monaghan, D. McAlpine, and Y. Zhang, "A survey on deep learning based brain computer interface: Recent advances and new frontiers," 2019, *arXiv:1905.04149*. [Online]. Available: https://arxiv.org/abs/1905.04149
[50] N. Naseer, M. J. Hong, and K.-S. Hong, "Online binary decision decoding using functional near-infrared spectroscopy for the development of brain–computer interface," *Exp. Brain Res.*, vol. 232, no. 2, pp. 555–564, Feb. 2014.
[51] Y. Kubota, N. N. Takasu, S. Horita, M. Kondo, M. Shimizu, T. Okada, T. Wakamura, and M. Toichi, "Dorsolateral prefrontal cortical oxygenation during REM sleep in humans," *Brain Res.*, vol. 1389, pp. 83–92, May 2011.
[52] J. W. Barker, A. Aarabi, and T. J. Huppert, "Autoregressive model based algorithm for correcting motion and serially correlated errors in fNIRS," *Biomed. Opt. Express*, vol. 4, no. 8, pp. 1366–1379, Aug. 2013.
[53] M. R. Bhutta, K.-S. Hong, B.-M. Kim, M. J. Hong, Y.-H. Kim, and S.-H. Lee, "Note: Three wavelengths near-infrared spectroscopy system for compensating the light absorbance by water," *Rev. Sci. Instrum.*, vol. 85, no. 2, Feb. 2014, Art. no. 026111.
[54] A. Zafar and K.-S. Hong, "Neuronal activation detection using vector phase analysis with dual threshold circles: A functional near-infrared spectroscopy study," *Int. J. Neural Syst.*, vol. 28, no. 10, Dec. 2018, Art. no. 1850031.
[55] J. Li and L. Qiu, "Temporal correlation of spontaneous hemodynamic activity in language areas measured with functional near-infrared spectroscopy," *Biomed. Opt. Express*, vol. 5, no. 2, pp. 587–595, 2014.
[56] H. Santosa, M. J. Hong, S.-P. Kim, and K.-S. Hong, "Noise reduction in functional near-infrared spectroscopy signals by independent component analysis," *Rev. Sci. Instrum.*, vol. 84, no. 7, Jul. 2013, Art. no. 073106.
[57] W. B. Baker, A. B. Parthasarathy, D. R. Busch, R. C. Mesquita, J. H. Greenberg, and A. G. Yodh, "Modified Beer–Lambert law for blood flow," *Biomed. Opt. Express*, vol. 5, no. 11, pp. 4053–4075, 2014.
[58] Q. C. Nguyen, M. Piao, and K.-S. Hong, "Multivariable adaptive control of the rewinding process of a roll-to-roll system governed by hyperbolic partial differential equations," *Int. J. Control, Autom. Syst.*, vol. 16, no. 5, pp. 2177–2186, Oct. 2018.
[59] H.-H. Kim, J.-K. Park, J.-H. Oh, and D.-J. Kang, "Multi-task convolutional neural network system for license plate recognition," *Int. J. Control Autom. Syst.*, vol. 15, no. 6, pp. 2942–2949, Dec. 2017.
[60] J. Ma, S. Ni, W. Xie, and W. Dong, "Deep auto-encoder observer multiple-model fast aircraft actuator fault diagnosis algorithm," *Int. J. Control Autom. Syst.*, vol. 15, no. 4, pp. 1641–1650, Aug. 2017.
[61] C. Bogler, J. Mehnert, J. Steinbrink, and J.-D. Haynes, "Decoding vigilance with NIRS," *PLoS One*, vol. 9, no. 7, Jul. 2014, Art. no. e101729.
[62] M. R. Bhutta, M. J. Hong, Y.-H. Kim, and K.-S. Hong, "Single-trial lie detection using a combined fNIRS-polygraph system," *Frontiers Psychol.*, vol. 6, Jun. 2015, Art. no. 709.
[63] N. Naseer and K.-S. Hong, "Decoding answers to four-choice questions using functional near infrared spectroscopy," *J. Near Infr. Spectrosc.*, vol. 23, no. 1, pp. 23–31, Jan. 2015.
[64] C.-S. Wei, Y.-T. Wang, C.-T. Lin, and T.-P. Jung, "Toward drowsiness detection using non-hair-bearing eeg-based brain-computer interfaces," *IEEE Trans. Neural Syst. Rehabil. Eng.*, vol. 26, no. 2, pp. 400–406, Feb. 2018.
[65] D. Qian, B. Wang, X. Qing, T. Zhang, Y. Zhang, X. Wang, and M. Nakamura, "Drowsiness detection by Bayesian-copula discriminant classifier based on EEG signals during daytime short nap," *IEEE Trans. Biomed. Eng.*, vol. 64, no. 4, pp. 743–754, Apr. 2017.
[66] D. Qian, B. Wang, X. Qing, T. Zhang, Y. Zhang, X. Wang, and M. Nakamura, "Bayesian nonnegative CP decomposition-based feature extraction algorithm for drowsiness detection," *IEEE Trans. Neural Syst. Rehabil. Eng.*, vol. 25, no. 8, pp. 1297–1308, Aug. 2017.
[67] C. Craye, A. Rashwan, M. S. Kamel, and F. Karray, "A multi-modal driver fatigue and distraction assessment system," *Int. J. Intell. Transp. Syst. Res.*, vol. 14, no. 3, pp. 173–194, 2016.

M. ASJID TANVEER received the B.S. degree in electrical engineering and computer sciences from the National University of Sciences and Technology (NUST), Islamabad, Pakistan, in 2018. He is currently a Research Associate with the National Center of Artificial Intelligence (NCAI), NUST, Pakistan.

M. JAWAD KHAN received the B.E. and M.S. degrees in mechatronics engineering from Air University, Pakistan, in 2007 and 2010, respectively, and the Ph.D. degree in mechanical engineering from Pusan National University, Busan, South Korea, in 2018. He worked on hybrid EEG-fNIRS-based brain–computer interfaces for rehabilitation, during his Ph.D. degree. He is currently an Assistant Professor with SMME, National University of Sciences and Technology (NUST), Pakistan. His research interests include hybrid brain–computer interfacing, rehabilitation, and machine learning.

M. JAHANGIR QURESHI received the bachelor's degree in mechatronics engineering. He is currently a Research Associate with Air University, Islamabad. His research interests include robotics, self-driving cars, natural language processing, deep learning, and machine learning.

NOMAN NASEER received the bachelor's, master's, and Ph.D. degrees in mechatronics engineering. He is currently the Head of the Neurorobotics Research Group, Air University, Islamabad. He has published more than 70 peer-reviewed articles. His research interests include robotic rehabilitation, biorobotics, neurorobotics, and machine learning. He has served as a Reviewer of more than 60 SCI(E) indexed journal articles. He is serving as an Editorial Board Member of three SCI(E) indexed journals.

KEUM-SHIK HONG received the B.S. degree in mechanical design and production engineering from Seoul National University, in 1979, the M.S. degree in mechanical engineering from Columbia University, New York, NY, USA, in 1987, and the M.S. degree in applied mathematics and the Ph.D. degree in mechanical engineering from the University of Illinois at Urbana–Champaign (UIUC), in 1991.

He joined the School of Mechanical Engineering, Pusan National University (PNU), in 1993. His Integrated Dynamics and Control Engineering Laboratory was designated a National Research Laboratory by the Ministry of Science and Technology of Korea, in 2003. In 2009, under the auspices of the World Class University Program of the Ministry of Education, Science and Technology of Korea, he established the Department of Cogno-Mechatronics Engineering, PNU. His current research interests include brain–computer interface, nonlinear systems theory, adaptive control, distributed parameter systems, and innovative control applications in brain engineering. He is a member of the National Academy of Engineering of Korea, a Fellow of the Korean Academy of Science and Technology, an ICROS Fellow, and many other societies. He has received many awards, including the Presidential Award of Korea, in 2007, the ICROS Achievement Award, in 2009, the Premier Professor Award, in 2011, the JMST Contribution Award, in 2011, the IJCAS Contribution Award, in 2011, and the IEEE Academic Award of ICROS, in 2016. He served as an Associate Editor of Automatica, from 2000 to 2006, as the Editor-in-Chief of the *Journal of Mechanical Science and Technology*, from 2008 to 2011. He is serving as the Editor-in-Chief of the *International Journal of Control, Automation, and Systems*. He was the past President of the Institute of Control, Robotics and Systems (ICROS), South Korea. He is the President of the Asian Control Association.